

# Nitrogen Glow Discharge by a DC Virtual Cathode

Azza M. Shager<sup>a</sup>, Amany T. Sroor<sup>b</sup>, Hoda A. El Tayeb<sup>a</sup>, Hoda A. El Gamal<sup>a</sup>,  
and Mohamed M. Masoud<sup>a</sup>

<sup>a</sup> Plasma Physics and Nuclear Fusion Department, Atomic Energy Authority, Cairo, Egypt

<sup>b</sup> Faculty of Girls, Ein Shams University, Cairo, Egypt

Reprint requests to M. M. M.; E-mail: mohmas65@yahoo.com

Z. Naturforsch. **63a**, 412–418 (2008); received May 26, 2006

A DC glow discharge operating with a virtual cathode is studied. The system consists of a solid disc cathode and mesh anode. The discharge occurs in nitrogen gas at the left-hand side of Paschen's curve. The plasma electron density in the axial direction has been found to be  $0.2 \cdot 10^8 \text{ cm}^{-3}$  at 2 cm from the mesh. The electron temperature peak value has been found to be 3.5 eV at 6 cm from the mesh. The radial distribution of the plasma electron density and temperature are discussed. The variation of the plasma parameters are in good agreement with the experimental results.

*Key words:* Glow Discharge; DC Virtual Cathode Oscillator; Vircator.

## 1. Introduction

Normal glow discharges exist at the right-hand side of Paschen's curve, and the discharge potential between the electrodes remains constant. The current can be varied by increasing the number of electrons from the cathode, which is due to the increase of the discharge area, while the current density is nearly constant. An increase in the current density is required in order to increase the total current, which will shift the normal discharge to the up-normal discharge region. In most previous work a virtual cathode oscillator was produced by a pulsed glow discharge plasma at the left-hand side of Paschen's curve. The accelerated electron beam crossing the mesh anode interacts with the formed plasma which generates microwaves. Many experimental studies have been carried out on the virtual cathode oscillator (vircator) in order to improve the total current [1–6] and to improve emitted microwave efficiency [7].

The vircator consists of a disk cathode and a mesh anode, connected to a power supply, which produces fast high-current pulses to form virtual cathode oscillators for high-power microwave production [8, 9]. Cathodic arcs have a similar construction [10]. A virtual cathode is formed when the electron beam current in the drift region exceeds the space charge-limiting current. Although the configuration of the virtual cathode oscillator is simple, the interaction between the electron beam and the oscillating field is complicated.

The mechanism of the virtual cathode discharge can be described as follows: The electrons emitted from the cathode surface are accelerated toward the mesh anode. The electrons will cross the mesh and form a virtual cathode where the mean free path for the collisions of the electrons is comparable or larger than the electrode separation [11]. The virtual cathode prevents the propagation of beam further downstream. Therefore most of the electrons are back reflected toward the anode. Only a small fraction of the electrons is allowed to propagate forward. The forward current increases as the diode gap increases. This is often called the current leakage [12]. In order to increase the electron energy and to improve the total current, the oscillation frequency between the real cathode and virtual cathode is increased. The oscillation frequency is optimal when the plasma frequency coincides with the electron cyclotron frequency.

In this study the discharge system consists of a solid disc cathode and a mesh anode similar to the pulsed virtual cathode oscillators for high-power microwave production [10, 11] or cathodic arcs but with low DC voltage and discharge current [10]. The virtual cathode is expected to be formed in the DC discharge, since the electron beam current in the drift region exceeds the space charge-limiting current.

## 2. Experimental

A virtual cathode DC glow discharge is composed of two electrodes enclosed by a discharge vessel, which is

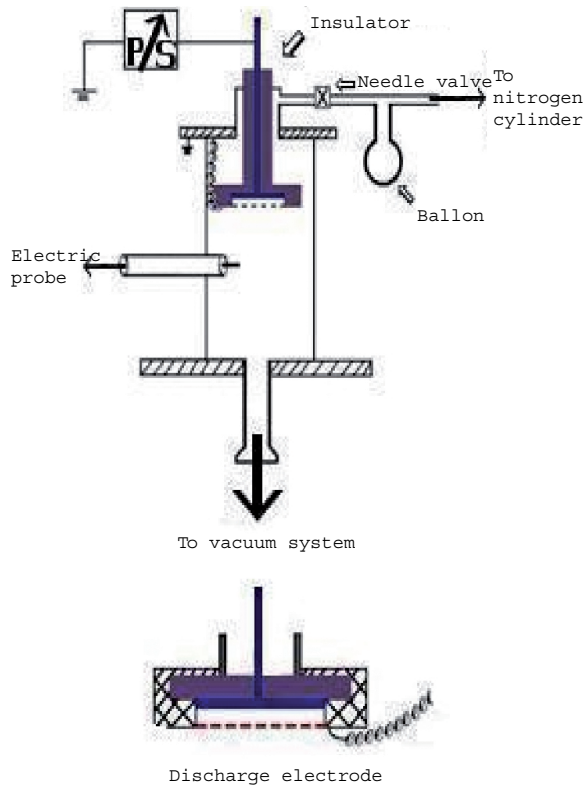


Fig. 1. Schematic diagram of the system.

made of Pyrex glass of 30 cm length and 10 cm diameter, respectively. It contains four ports in the middle of the vessel for introducing the different diagnostic tools. The Pyrex vessel was evacuated to a basic pressure of  $10^{-3}$  Torr. The nitrogen gas was leaked through a needle valve to keep a constant working gas pressure at 10 Torr.

The virtual cathode DC glow discharge consists of a brass in the form of a mesh, which acts as anode, and of a copper disc cathode. The anode and cathode are fixed together by a rod of copper to fix the spacing between them to 4 mm. The system can move freely in axial direction through the glass cylinder by moving it up and down. Figure 1 illustrates the experimental setup. The cathode is connected to the negative potential of a DC power supply, which can be adjusted to the desired voltage, while the anode is connected to the earth.

An electric probe is made from tungsten with a diameter of 0.5 mm and a length of 5 mm. It is inserted through the port in the middle of the discharge vessel via a vacuum-sealed system to move freely in the radial direction. The plasma electron temperature  $T_e$  is calculated from the slope of the logarithm of the electric

probe current versus probe voltage and from the electron energy distribution function (EEDF). The electron density is calculated using the relation

$$I_{es} = n_e A e (kT_e / 2\pi m_i)^{1/2},$$

where  $n_e$  is the electron density,  $A$  the probe's surface area,  $k$  the Boltzman constant,  $m_i$  the ion mass,  $e$  the electron charge, and  $T_e$  the electron temperature.

### 3. Results

To understand the behaviour of the discharge, the electrical parameters have been measured. Figure 2 shows the variation of voltage applied between the mesh anode and the disk cathode and the current through the system. The figure shows the characteristic curve of a discharge. The discharge starts at 430 V, and the corresponding current did not exceed several mA. It has been found that the discharge current increases with increasing the potential between the mesh anode and the disc cathode, according to the relation  $V \propto I^{3/2}$ .

Paschen's curve for nitrogen gas is presented in Fig. 3; the discharge current is in mA and the separation gap between the electrodes is 4 mm. The relation between the breakdown potential  $V_B$  and the pressure factor  $pd$  has been presented by von Engel as  $V_B = C_1(pd)/C_2 + \ln(pd)$ , where  $C_1$  and  $C_2$  are constants, which depend on the type of the working gas [13].

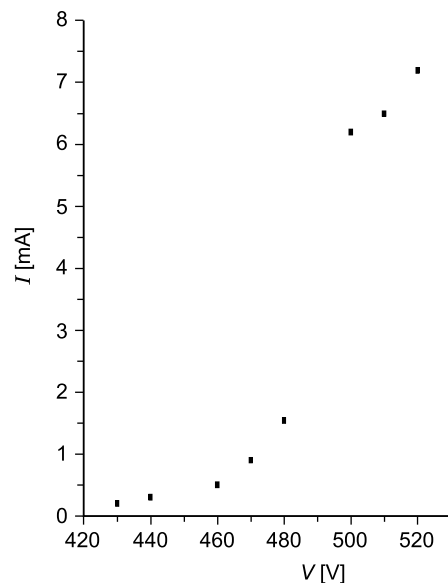


Fig. 2. Voltage-current characteristic curve.

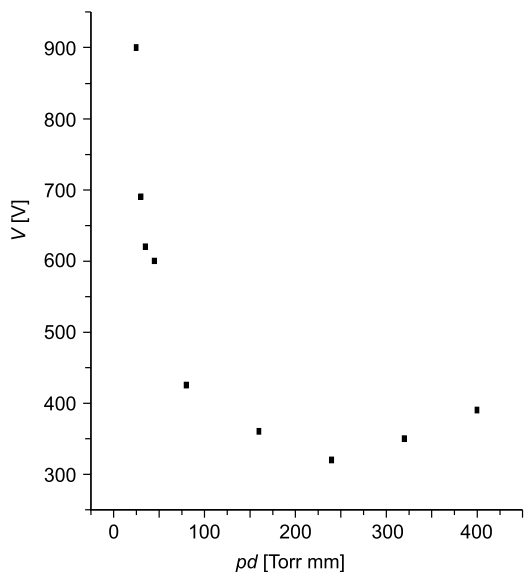


Fig. 3. Paschen curve breakdown voltage  $V$  versus  $pd$  for  $N_2$ .

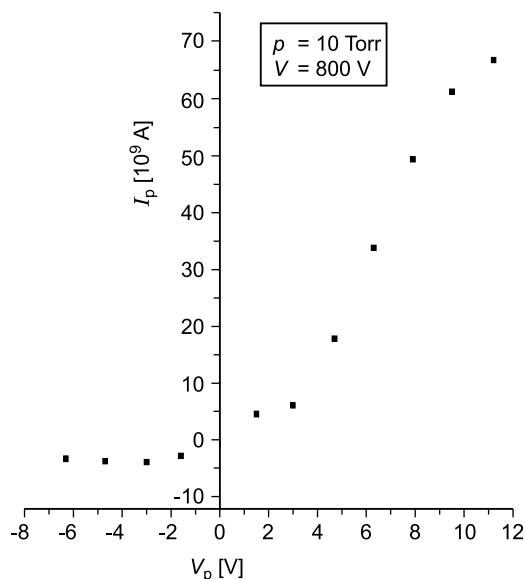


Fig. 4. Characteristic curve of the electric probe.

Apparently at higher  $pd$  values (above 1.2 Torr cm) the breakdown voltage between two electrodes is proportional to  $pd$  [14]. Figure 3 shows that the breakdown potential decreases rapidly with increasing pressure until it reaches its minimum of 325 V at  $pd \approx 1.2$  Torr cm. The left-hand side of the curve provides the suitable condition for this experiment, since the electron-atom collision mean free path is greater than the electrode separation distance. Hence for  $pd =$

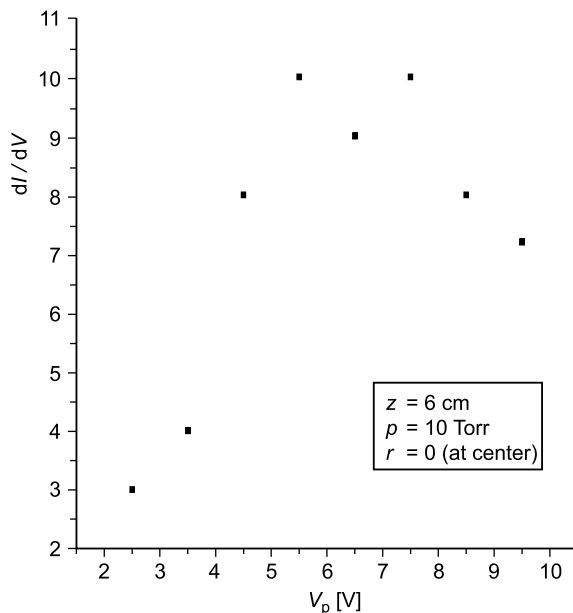


Fig. 5. First derivative  $dI/dV$ .

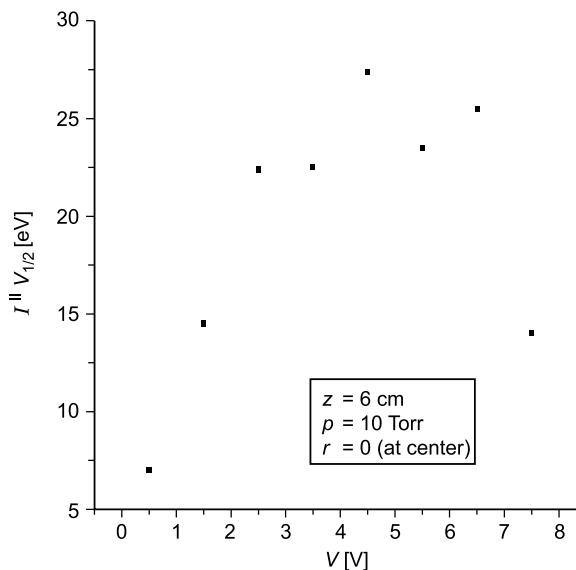


Fig. 6. Electron energy distribution.

1 Torr cm the virtual cathode will be formed as a result of the collisions between the electrons and the neutral atoms outside of the two electrodes.

To measure the plasma parameters such as the electron temperature, the plasma density, and the electron energy distribution function, which are produced by the virtual cathode DC glow discharge, a single electric probe is used [15, 16]. In Fig. 4 the electric probe

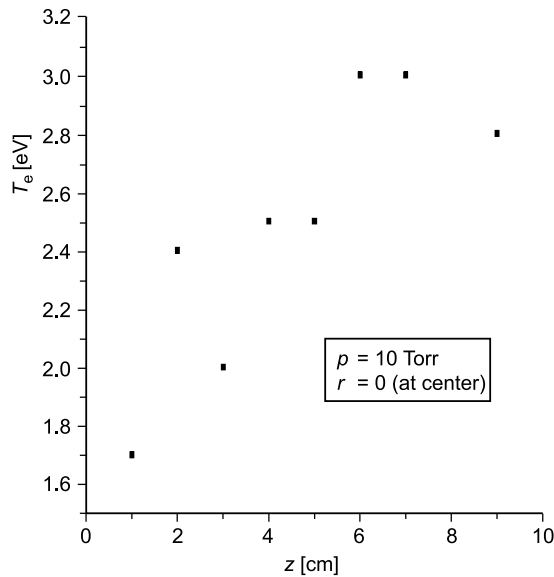


Fig. 7. Axial distribution of the electron temperature.

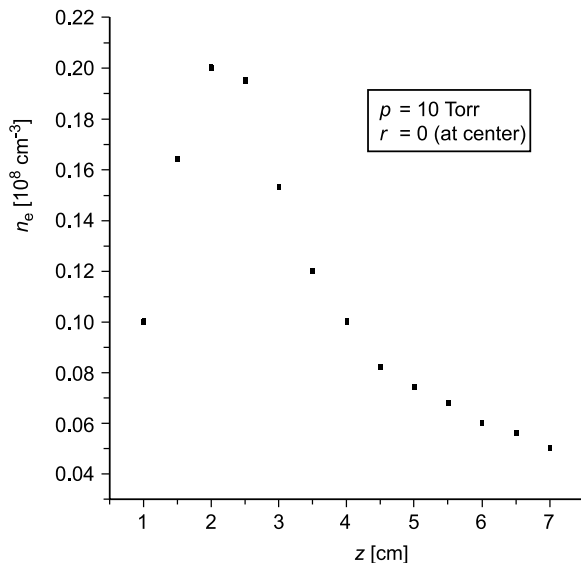


Fig. 8. Axial distribution of the electron density.

current  $I_p$  is plotted against the applied voltage  $V_p$  to obtain the characteristic curve at an axial distance  $z = 6$  cm, at  $r = 0$  (at center), pressure  $p = 10$  Torr, and discharge current 5 mA. Figure 5 shows the dependence of the first derivative  $dI/dV$  on the probe voltage. From this curve we notice that  $dI/dV$  increases with increasing probe voltage to reach its maximum value at  $V_p \approx 7$  V, which is the plasma potential; then it decreases rapidly to its minimum value  $\sim 0$ , at  $V_p \approx 15$  V.

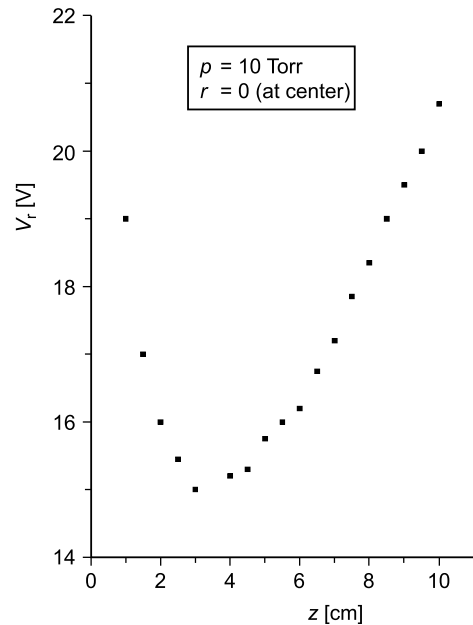


Fig. 9. Axial distribution of the plasma potential.

Figure 6 shows the EEDF under the above conditions. The peak temperature turns out to be about 4 eV. The EEDF curve is similar to the Maxwellian distribution expected from theory. Figure 7 shows the axial distribution of the electron temperature. We observe that it increases along the tube axis  $z$  to reach its highest rate (3.5 eV) at the distance  $z = 6$  cm. At axial distance more than 6 cm, the electron temperature starts to decrease, which can be attributed to the weaker electric field and the diffusion of the charged particles.

The axial distribution of the electron density is illustrated in Figure 8. Note that the electron density increases with axial direction from the mesh to reach its maximum value  $0.2 \cdot 10^8 \text{ cm}^{-3}$  at  $z = 2$  cm. This may be due to an increase of the electron beam collisions, which increases the ionized particles, forming the virtual cathode (negative glow region) around 2 cm from the mesh. The number of electrons for  $z$  larger than 2 cm from the mesh then decreases.

Figure 9 presents the axial distribution of plasma potential  $\phi$  obtained from the first derivative of the probe's characteristic curve  $I_p$  versus  $V_p$  at different axial positions. From the curve we observe that the plasma potential decreases from the grid anode to reach its minimum value nearly 15 V at  $z = 3$  cm. The region near the minimum potential can be defined as the virtual cathode. Furthermore this figure shows that

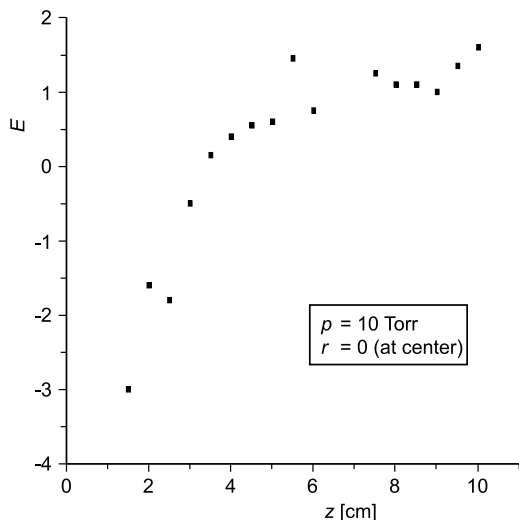


Fig. 10. Axial distribution of the electric field.

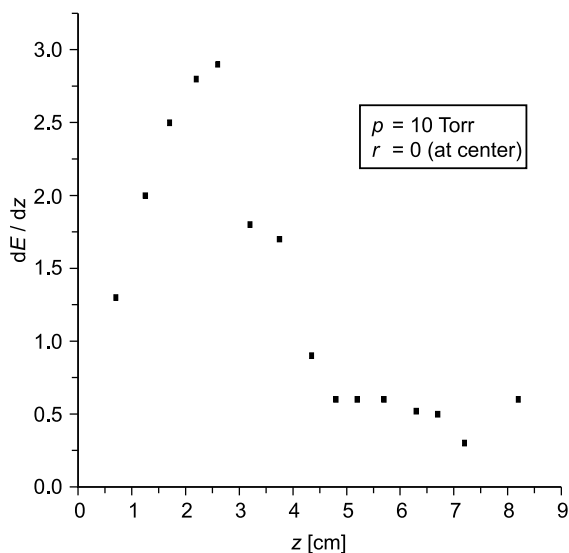


Fig. 11. Axial distribution of the plasma density.

for an axial position of 3 cm from the mesh the plasma potential increases rapidly, which may represent an expanding plasma column.

The axial electric field ( $E$ ) distribution has been calculated from the potential ( $\phi$ ) distribution,  $E = -\text{grad } \phi$ , as shown in Figure 10. The electric field profile clearly shows the direction of the electric field if  $z$  is less than 3 cm. We attribute this to the forward-accelerated electron current. The electric field reverses its direction after 3 cm. Then it has a nearly constant and rather low value, which may be interpreted as part of the backward current.

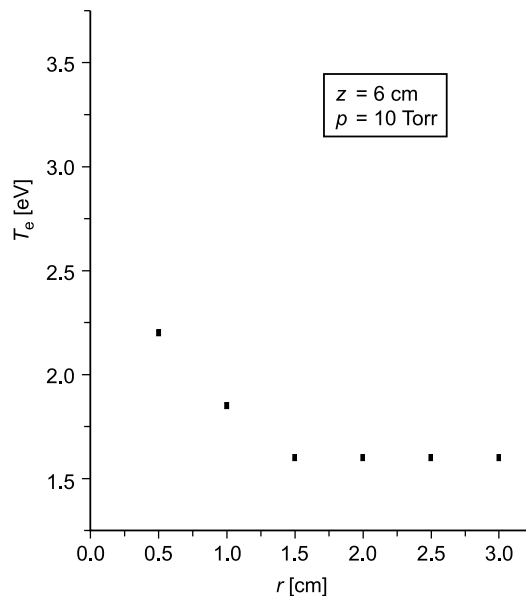


Fig. 12. Radial distribution of the electron temperature.

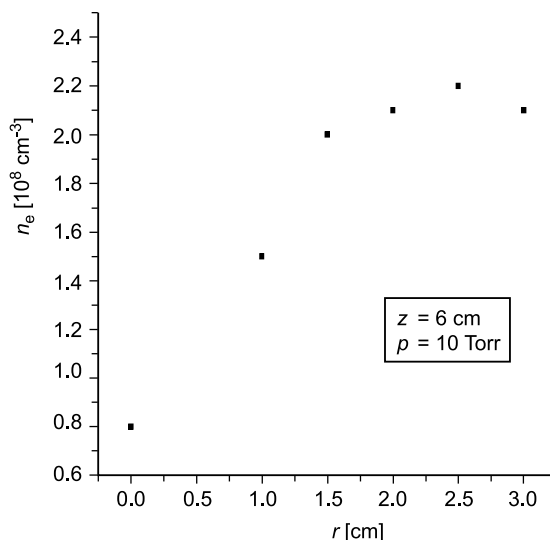


Fig. 13. Radial distribution of the electron density.

Figure 11 shows the calculated plasma density  $dE/dz$  along the  $z$ -axis. From the curve we notice that the plasma density changes along the tube axis, where the electric field generated by the beam's space charge is related to the electron density by the Poisson equation

$$\Delta^2 \phi = \epsilon \rho = \text{div} E = -d^2 \phi / dz^2.$$

Here  $E$  is the electric field,  $\rho$  the electron density,  $\epsilon$  the permittivity in  $\text{F m}^{-1}$ , and  $z$  the axial coordinate.

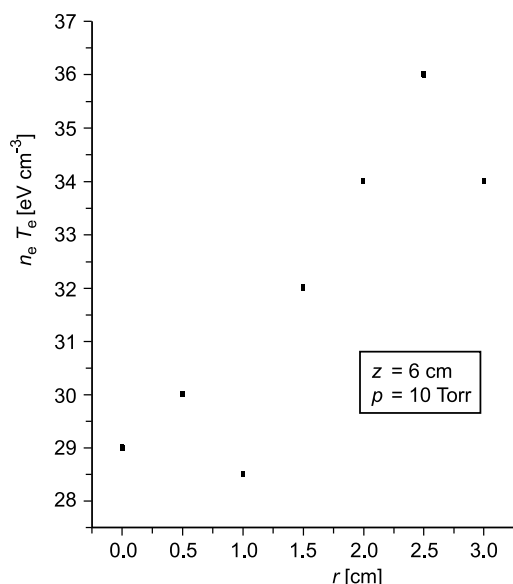


Fig. 14. Radial distribution of the plasma kinetic energy.

The position of the virtual cathode has been estimated to be at about 3 cm from the grid, which can be confirmed from the change of electric field's changing of its direction as well as from the peak plasma density at that position.

Figure 12 shows the radial distribution of the electron temperature at  $z = 6$  cm, nitrogen gas pressure  $p = 10$  Torr, and with discharge current  $I = 5$  mA. It is clear from this figure that the electron temperature has a maximum value of  $T = 3.5$  eV at the center of the tube, and it decreases rapidly from the center up to  $r \sim 1.5$  cm; then it has a nearly constant level of 1.6 eV until near the tube wall. This means that the accelerated electron beam is concentrated around the center

with small dispersion, where only the diffusion of the electron energy toward the discharge wall takes place.

The radial distribution of the electron density is shown in Figure 13. From this curve we see that the electron density increases rapidly from the center toward the wall, and reaches its maximum value  $2.2 \cdot 10^8$  cm<sup>-3</sup> at  $r = 2.3$  cm from the center; then it decreases.

Figure 14 finally shows the change of the plasma kinetic energy ( $nkT$ ) with radial direction. It is clear that the kinetic energy increases along the radial direction to its maximum value at  $r = 2.5$  cm and then decreases towards the wall. This is due to diffusion to the wall.

#### 4. Conclusion

A new type of DC glow discharge originating from a virtual cathode using nitrogen gas has been studied. The system consists of a disc cathode and a mesh anode. The discharge takes place at the left-hand side of Paschen's curve. The plasma electron density in the axial direction has a peak value of  $\rho = 0.2 \cdot 10^8$  cm<sup>-3</sup> at  $z = 2$  cm from the mesh. The electron temperature has a peak value of  $kT_p = 3.5$  eV at  $z = 6$  cm from the mesh. It has been found that the electron energy has Maxwellian distribution function to good approximation. The experimental values of the electron density agree with the calculated theoretical one from the plasma potential (Poisson equation). The variation of the plasma potential in axial direction is obtained and the corresponding theoretical plasma parameters are in good agreement with the experimental results, especially the position of the virtual cathode.

- [1] S. C. Burkhart, R. D. Scarpetti, and R. L. Lundberg, *J. Appl. Phys.* **58**, 28 (1985).
- [2] M. Haworth, R. Adler, B. Anderson, M. Connaughton, W. Dungan, J. Enns, J. Metz, P. Pelletier, R. Platt, J. Polaco, R. Rupp, L. Thodes, and D. Voss, *Appl. Phys. Lett.* **59**, 408 (1991).
- [3] H. A. Davis, R. R. Bartsch, T. J. T. Kwan, E. G. Sherwood, and R. M. Stringfield, *Phys. Rev. Lett.* **59**, 288 (1987).
- [4] W. Jiang, H. Kitano, L. Huang, K. Masugata, and K. Yatsui, *IEEE Trans. Plasma Sci.* **24**, 187 (1996).
- [5] W. Jiang, K. Woolverton, J. Dickens, and M. Kristiansen, *IEEE Trans. Plasma Sci.* **27**, 1538 (1999).
- [6] W. Jiang, J. Dickens, and M. Kristiansen, *IEEE Trans. Plasma Sci.* **27**, 1538 (1999).
- [7] W. Jiag and M. Kristiansen, *Am. Inst. Phys.* **8**, 8 (2001).
- [8] C. D. Taylor and D. V. Giri, *High-Power Microwave Systems and Effects*, Taylor & Francis, New York 1994, p. 7.
- [9] W. Jiang, K. Masagata, and K. Yatsui, *Phys. Plasmas* **2**, 982 (1994).
- [10] T. Zhang, B. Tang, Z. Zeng, Q. Chen, and P. K. Chu, *IEEE Trans. Plasma Sci.* **27**, 786 (1999).
- [11] J. Urban and K. Frank, *Spectroscopic investigations of the plasma of a pseudospark discharge*, in: *Proceedings of the XXV ICPIG Japan, 2001*, Vol. 4, p. 203.

- [12] H. S. Uhm, E. H. Choi, and M. C. Choi, *Am. Inst. Phys.* **79**, 7 (2001).
- [13] A. von Engel, *Electric Plasmas, their Nature and Uses*, Taylor and Francies, London and New York 1983.
- [14] M. Sato, *Bull. Yamagata Univ.* **25**, 119 (1999).
- [15] N. A. Krall and A. W. Trivelpiece, *Principles of Plasmas, Physics*, McGraw-Hill, New York 1973.
- [16] S. Glasston and R. H. Lovberg, *Controlled Thermonuclear Reaction*, Van Nostrand, Princeton 1960.